Interaction between transition metals (Co, Ni, and Cu) systems and amorphous silica surfaces: A DFT investigation

Saber Gueddida, Sébastien Lebègue, Michael Badawi

Interaction between transition metals (Co, Ni, and Cu) systems and amorphous silica surfaces: a DFT investigation

Saber Gueddida[a,*], Sébastien Lebègue[a], Michael Badawi[a,*]

[a] *Univ. Lorraine, LPCT, CNRS UMR7019, F-54506 Vandoeuvre-Les-Nancy, France.*

Abstract

Transition metals (Co, Ni, or Cu) systems supported on amorphous silica are promising materials for their unique surface chemical reactivity. Despite many investigations, the transition metal-support interactions for this type of materials are not yet well understood at the molecular level. In this work, periodic density functional theory calculations, were performed to investigate systematically the interaction between Co, Ni, or Cu species (monomers and clusters) and amorphous silica surfaces with densities of 3.3 and 4.6 OH/nm^2. It is shown that the geometry, energetic stability, and magnetic properties of transition metal species deposited on amorphous silica surfaces depend strongly of the number of M-O-Si groups and, in few cases, of the number of M-OH-Si groups, with sometimes a strong effect on the silica surface that induces a reorganization of the silanol groups. Among monomers, cobalt is found to be the most stable on the silica surface while among clusters, the Ni cluster is the most strongly adsorbed. The magnetic moments of the adsorbed transition metal clusters on silica surface are found to be reduced with respect to their corresponding free clusters for Co and Ni.

Keywords: DFT, silica, nanoparticles, clusters, single site, catalyst.

1. Introduction:

Transition metal based catalysts are of uttermost importance for many important chemical processes, such as ethene polymerization [1, 2], dehydrogenation of alkanes [3, 4, 5, 6], selective oxidation reactions [7, 8, 9], and hydrodeoxygenation (HDO) reaction [10, 11, 12, 13, 14, 15, 16, 17]. The most common supports are silica-based materials (silica and zeolites), alumina and titania due to their specific physico-chemical properties and also to their abundance and relatively low price [18, 19, 20]. Due to its mechanical resistance, high dielectric strength, and selectivity for chemical modification, amorphous silica(SBA-15, MCM-41 and analogous formulations) stands as one of the most important support used today [21, 22, 23, 24, 25]. In particular, amorphous silica materials containing Co, Ni, or

*I am corresponding author
Email addresses: saber.gueddida@univ-lorraine.fr (Saber Gueddida), michael.badawi@univ-lorraine.fr (Michael Badawi)

Cu (as atomically dispersed or cluster-shaped) have a wide range of catalytic applications implying reactions such as hydrogenation, hydrogenolysis, hydrodeoxygenation, various process involved in expanding the energy resources, Fischer-Tropsh synthesis, reforming, and water-gas-shift [26, 27, 28, 29].

The design of catalysts strongly depends on the type and size of the supported nanoparticles, which outstandingly improve the catalytic activity and extend the catalyst life even when small amounts are grafted. Recently, it has been shown experimentally that the use of SBA-15 containing residual hydrophilic groups is efficient to control the size and localization of Cu nanoparticles that could be extended to other mono- or bi- component transition metal nanoparticles loaded on mesoporous silica, such as those based on Ni, Co, Fe, or Mn [28]. The catalytic activity of Ni/SBA-15 materials in the hydrogenation reaction of cinnamaldehyde is significantly increased when the very small nickel particles are located in the silica intra-wall micropores, because the metal phase dispersion is high and the diffusion of the reactants is facilitated in the mesopores of the support [29, 26, 27]. Also, cobalt and nickel have shown a promoting effect on the activity of hydrotreating catalysts in the hydrogenation and the isomerization of olefins [30, 31].

From a more fundamental point of view, transition metal nanoparticles can form monomers, dimers, and clusters on silica. Several studies reported that transition metal nanoparticles made of 13 atoms show a particularly large stability [32, 33, 34, 35]. Transition metal clusters have experimentally been found to have a dominant structural characteristic of icosahedral symmetry. The calculations of the bonds lengths and the binding energies of the free small transition metal clusters show that the most stable structure is the icosahedral cluster with n = 13 atoms. The determining factor of a high stability of this structure is the bond symmetry, i.e., the presence of the maximum number of the nearest atoms [35]. Atoms in the icosahedron geometry (13 atoms) have the maximum number of the nearest neighboring atoms and the distance between the nearest atoms is the same. This "magic" cluster also exhibits a high dynamic stability which is characterized by significant degeneracy of the vibration amplitudes of the cluster. Most of earlier theoretical studies [36] were based only on an icosahedral geometry, where it has been successfully applied to represent the interaction between transition metal atoms (such as impact, surface, and boundary layer). On the other hand, it has been shown experimentally that the transition metal nanoparticles (such as Ni) of size reaching 11nm are observed on SBA-15, but the nanoparticles population is centered at 4-5 nm, with an average nanoparticles size calculated at 5.1 nm [29, 26, 27, 28], which corresponds to the size of the icosahedral geometry (13 atoms).

Computational studies can provide complementary informations not accessible by experimental techniques [18, 23, 37, 38]. However, a realistic modeling of heterogenous catalysts containing amorphous supports remains a challenge [39, 23]. To the best of our knowledge, the interaction between the transition metal (Co, Ni, Cu) species and the amorphous silica surfaces has not yet been studied by ab initio methods, which would be helpful to optimize the formulation of catalytic nanomaterials. The aim of the present work is therefore to elucidate the different grafting modes and the electronic and magnetic properties of different transition metal species (isolated monomers and clusters) on various amorphous silica-surfaces.

This paper is organized as follows: In the first section we briefly describe our calculation methods, and in second section we present our results for the supported Co, Ni, and Cu monomers and clusters on amorphous hydroxylated surfaces. We first describe the structural properties of different grafting structures of different transition metals and then discuss their electronic and magnetic properties. Finally, we offer our conclusions and perspectives.

2. Computational Details

The periodic spin polarized density functional theory (DFT) calculations reported in this work were carried out using the Vienna *Ab Initio* Simulation Package (VASP) [40] using the projector augmented wave method (PAW) [41]. The exchange and correlation potential was accounted for within the generalized gradient approximation using the functional of Perdew, Burk and Ernzerhof(GGA-PBE) [42]. The rotationally invariant PBE+U correction [43, 44] was used in this work in order to properly describe the $3d$ states in transition metals (Co, Ni, and Cu), which tends to be inaccurately represented in standard DFT-PBE. All the systems containing d-metals Co, Ni, and Cu were calculated within the PBE+U approach with the Hubbard parameters U and J equal to 3 eV and 0.9 eV, respectively. The weak van der Waals interactions between transition metals and the silica surface were included within the Grimme approximation (DFT-D2) [45], as implemented in VASP [46].

In this work, we have investigated the interaction between different transition metals species and two amorphous silica surfaces which present silanol densities of 3.3 and 4.6 OH/nm^2, respectively (denoted hereafter SiO_2-3.3 and SiO_2-4.6). These densities correspond to those found in mesoporous silica experimental samples [47, 48, 49, 50, 51, 52]. The considered surfaces have been constructed by Comas-Vives via the dehydroxylation of a fully hydroxylated surface [53] using a periodic supercell containing 375 atoms for SiO_2-3.3 and 384 atoms for SiO_2-4.6. In all cases, we used more than 20 Å of vacuum in the z direction to separate the periodically repeated slabs. The lattice parameters for these periodic structures are a = b = 21.39 Å, c = 34.17 Å, and $\alpha = \beta = \gamma = 90°$ [53]. The transition metal clusters have been modeled using 13 atoms [32, 33, 34, 35]. These structures show the most stable atomic arrangement among small clusters of series of transition metals such as Co_{13}, Ni_{13}, and Cu_{13}, and adopt the D_{3d} symmetry. The particular structural stability of the 13-atoms cluster is observed also for other nanoparticles such as Fe_{13} [54], Ga_{13} [55] or Pt_{13} [56]. The energy cutoff of the plane waves was set to 450 eV. For integration within the Brillouin zone, only the Γ point was selected for all calculations due to the large size of the supercell. The convergence criterion of the total energy differences was set to 10^{-6} eV. For geometry optimization, the positions of the single transition metal atoms (M = Co, Ni, Cu) or all the atoms of the M_{13} cluster and those of the first plane of the silica substrate (Si, O, and H atoms) were relaxed while keeping the other planes fixed. The force criterion was set to 0.03 eV/Å. A Bader charge analysis [57, 58] of M_{13}/SiO_2 calculated with PBE+U+D2 method has been applied to determine the charge transfer between the M_{13} clusters and the amorphous silica surfaces. The Bader charge analysis was performed using the reconstructed valence density in the PAW formulation [59] with a 180 × 180 × 280 density grid with a charge transfer error estimated to be around ± 0.01 e^-.

3. Results and discussion

3.1. Supported transition metal monomers

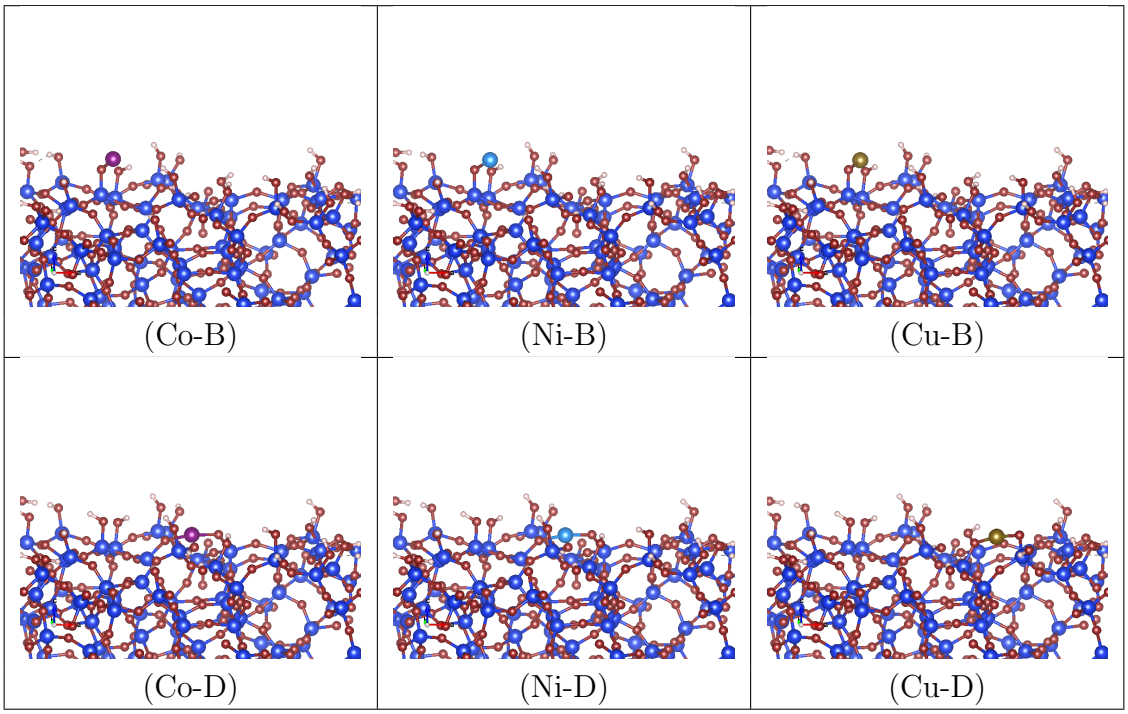

Figure 1: The most stable structures of the supported single Co (left panels), Ni (middle panels), and Cu (right panels) atoms on amorphous silica surface SiO_2 with a silanol density equal to 4.6 OH/nm^2 at top (M-B cases) and bridge (M-D cases) positions, respectively: Co atoms in violet, Ni atoms in cyan, Cu atoms in gold, Si atoms in blue, O atoms in brown and H atoms in white.

Before finding the most stable structures of M_{13}/SiO_2, different geometrical configurations of supported transition metal monomers on silica surfaces were systematically investigated within the PBE+U+D2 approximation. The single transition metal atom is adsorbed on the silica-surface through its oxygen atoms by removing the corresponding hydrogen atoms to allow the formation of M-O-Si bonds. The optimized structures show that the transition metal atom is grafted at the top (mono-grafting, hereafter named M-A and M-B) and the bridge (di-grafting, hereafter named M-C and M-D) positions and therefore one or two M-O-Si groups are established, respectively (see Figure 1).

Table 1 shows the calculated M-O bond lengths for the most stable grafting structures (top and bridge) of single transition metal atom on the SiO_2-4.6 and the SiO_2-3.3 silica surfaces. For the top oxygen sites, the bond length of the most stable structure (M-B) of Co/SiO_2-4.6 is 1.85 Å, while for Ni/SiO_2-4.6 and Cu/SiO_2-4.6, are 1.83 Å and 1.84 Å, respectively. These distances are slightly reduced when the single transition metal is adsorbed on the SiO_2-3.3 surface. However, the most stable bridge grafted structure (M-D) on SiO_2-3.3 or SiO_2-4.6 has M-O bond lengths in the range of 1.74-1.77 Å.

Table 1: PBE+U+D2 calculated equilibrium distance d_{M-O} (in Å) between the single transition metal atom (Co, Ni, and Cu) and the silica-surface with a silanol density of 4.6 or 3.3 OH/nm^2.

Structure	M/SiO_2-4.6			M/SiO_2-3.3		
	Co	Ni	Cu	Co	Ni	Cu
M-A	1.77	1.75	1.78	1.78	1.76	1.78
M-B	1.85	1.83	1.84	1.83	1.76	1.83
M-C	1.80-1.81	1.76-1.77	1.81-1.81	1.79-1.80	1.77-1.78	1.79-1.80
M-D	1.77-1.77	1.74-1.75	1.75-1.77	1.77-1.78	1.73-1.75	1.77-1.78

The single transition metal atom is grafted by dehydrogenation of surface silanols, following the reaction:

$$M + SiO_2(H_2)_m \rightarrow MSiO_2(H_2)_{m-\frac{n}{2}} + \frac{n}{2} \times H_2, \quad (1)$$

where n is the number of hydrogens removed from the surface and varied between 1 and 2 for top and bridge positions, respectively, and m is the number of H_2 of the silica-surface, 26 for SiO_2-4.6 and 23 for SiO_2-3.3. The adsorption energy ΔE is given by $\Delta E = E_{sys} + \frac{n}{2}E_{H_2} - E_{surf} - E_M$, where E_{sys} is the total energy of the whole system ($MSiO_2(H_2)_{m-\frac{n}{2}}$), E_{surf} and E_M are that of the free silica-surface and the transition metallic atom (M = [Co, Cu, Ni]), respectively, and E_{H_2} is that of H_2. The corresponding grafting energies are reported in Table 2 of a supported single transition metal atom on the amorphous silica-surfaces SiO_2-4.6 and SiO_2-3.3 for both top and bridge grafted structures. For Co/SiO_2-4.6, the calculated adsorption energies according to the reaction 1 are found to be -2.77 eV for the most stable top-grafted structure (Co-B) and -3.18 eV for the bridging oxygen sites, while for Co/SiO_2-3.3, are slightly reduced to -2.57 eV and -3.13 eV, respectively. The most stable configuration of the top and bridge modes of Ni/SiO_2-4.6 are the structures Ni-B and Ni-D with energy values of -2.24 eV and -2.42 eV, respectively, and -1.73 eV and -2.30 eV for Ni/SiO_2-3.3. However, for Cu/SiO_2-4.6, the grafting energies are found to be -2.42 eV and -1.09 eV for the most stable top and bridge-grafted structures, respectively, while for Cu/SiO_2-3.3, they are slightly reduced to -1.82 eV and -1.10 eV. Our calculations show that the most stable structure is predicted to be the M-D bridge site for Co/SiO_2 and Ni/SiO_2 and the M-B top site for Cu/SiO_2 system. The grafting energies of the supported transition metal on amorphous silica surface are in the order $\Delta E_{Co/SiO_2}$ (-3.18 eV) < $\Delta E_{Ni/SiO_2}$ (-2.42 eV) < $\Delta E_{Cu/SiO_2}$ (-2.03 eV), showing that cobalt atom interacts much more with the silica surface than nickel and copper.

For the top adsorption structure, the magnetic moment of the isolated cobalt atom is

Table 2: PBE+U+D2 calculated grafting energies (in eV) for an adsorbed single transition metal atom (Co, Ni, and Cu) on amorphous silica surfaces SiO_2-4.6 and SiO_2-3.3 at top (structures: M-A and M-B) and bridge (structures: M-C and M-D) positions.

Structure	M/SiO_2-4.6		M/SiO_2-3.3	
	ΔE	Ion	ΔE	Ion
Co-A	-1.86	Co^{3+}	-1.90	Co^{3+}
Co-B	-2.77	Co^{3+}	-2.57	Co^{3+}
Co-C	-2.51	Co^{2+}	-2.39	Co^{2+}
Co-D	-3.18	Co^{2+}	-3.13	Co^{2+}
Ni-A	-1.21	Ni^{2+}	-1.23	Ni^{2+}
Ni-B	-2.24	Ni^{2+}	-1.73	Ni^{2+}
Ni-C	-1.76	Ni^{3+}	-1.62	Ni^{3+}
Ni-D	-2.42	Ni^{3+}	-2.30	Ni^{3+}
Cu-A	-1.17	Cu^{2+}	-1.20	Cu^{2+}
Cu-B	-2.03	Cu^{2+}	-1.82	Cu^{2+}
Cu-C	-0.53	Cu^{+}	-1.09	Cu^{+}
Cu-D	-1.09	Cu^{+}	-1.10	Cu^{+}

found to be 1.90 μ_B, and 2.60 μ_B for the bridging oxygen sites which correspond to the high-spin magnetic moment of Co^{2+} and Co^{3+}, respectively. For both cases, we found a small positive magnetic moment induced on the oxygen atoms in direct contact with the cobalt atom of 0.02 μ_B and [0.13, 0.13] μ_B, respectively. For Ni/SiO_2, the magnetic moment of the isolated nickel atom is found to be 0.95 μ_B and 1.56 μ_B grafted at top and bridge positions, respectively, which correspond to Ni^{2+} and Ni^{3+} ions, while those induced on oxygen atoms are 0.04 μ_B and [0.16,0.16] μ_B, respectively. However, the magnetic moment of Cu^{+} (top grafting site) is zero, and that of Cu^{2+} (bridge grafting site), 0.50 μ_B. The induced magnetic moments of the last configuration are found to be [0.18,0.19] μ_B.

To conclude, our results show the stabilization of the Co and the Ni single sites on amorphous silica surfaces (SiO_2-4.6 and SiO_2-3.3) through both mono- and bridge grafting modes compared to the copper one. The calculated grafting energies show that the supported single cobalt atom is the most stable structure (Co-D structure). These results are in agreement with the high resolution TEM images which provide direct evidence that small

nanoparticles (< 2nm) of Ni and Co encapsulated inside the secondary pore network of SBA-15 showing an excellent thermally stability up to 900°C (oxidizing/reducing atmospheres) [29, 26, 27]. However, the experimental results indicated that the mobility of the copper species of such size (below 10 nm) makes them difficult to be stabilized on the surface of a solid support such as silica [28]. In situ reduction XRD experiment confirms the maintaining of low size nanoparticles even in metallic state, with a mean nanoparticles size evaluated in the TEM images always at $\sim$ 2 nm. XPS analysis was performed to evaluate the effect of the presence of the template of the final state of the transition metal on the material surface, showing the formation of Co^{2+} ions on the material surface, in strong interaction with the silica surface.

3.2. Adsorption of transition metal clusters

3.2.1. Structural properties

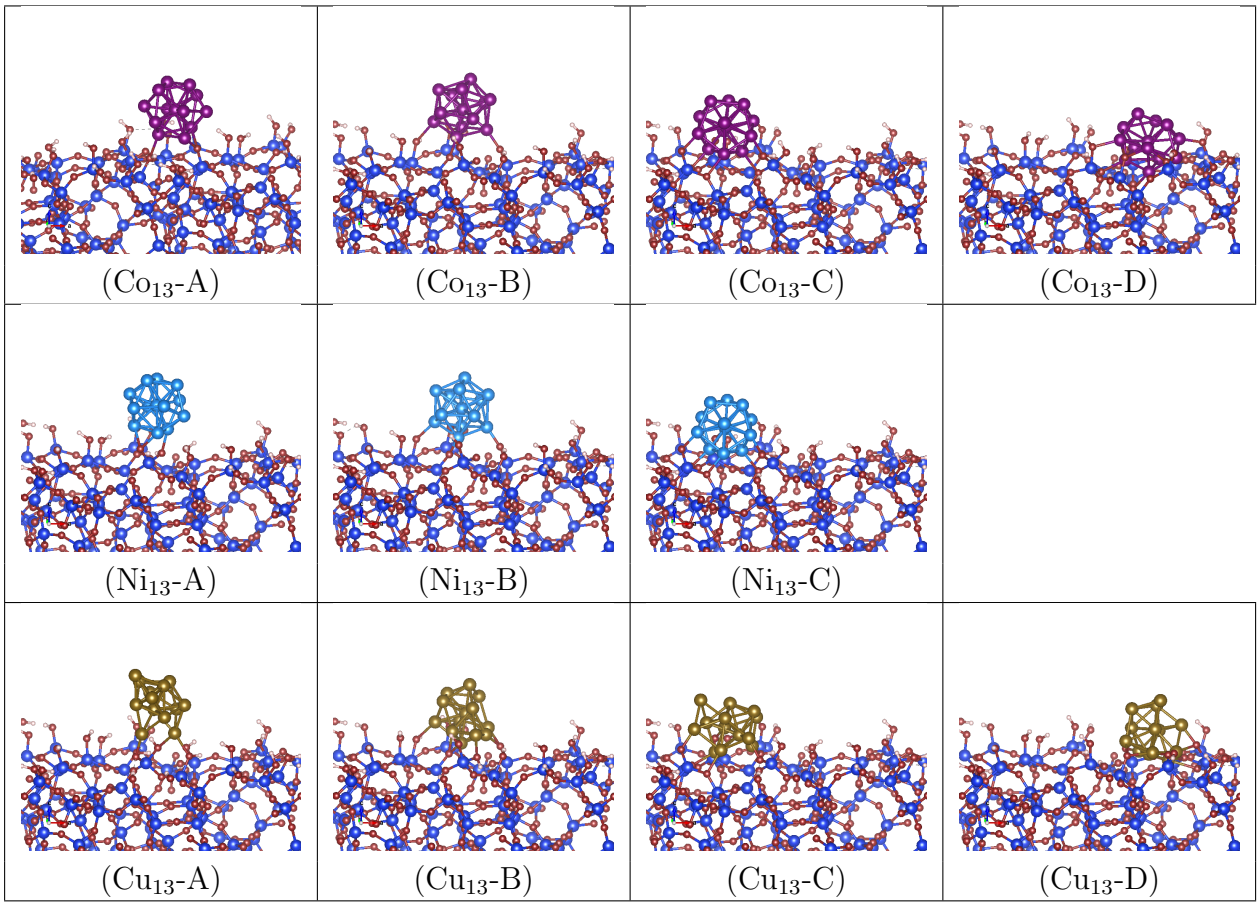

Figure 2: The most stable structures (M_{13}-A, M_{13}-B, M_{13}-C, and M_{13}-D) of the supported transition metal clusters (Co: upper, Ni: middle, and Cu: lower) on an amorphous silica surface having a silanol density of 4.6 OH/nm^2.

Several geometrical optimizations were started from reasonable guesses with various adsorption structures (mono- (M_{13}-A), di- (M_{13}-B), tri- (M_{13}-C), and tetra-grafting (M_{13}-D))

on SiO_2-3.3 and SiO_2-4.6 surfaces, in order to investigate the interaction between the transition metal cluster (Co_{13}, Ni_{13}, and Cu_{13}) and the amorphous silica-surface. It should be mentioned that for the SiO_2-3.3 surface, only the three first structures were investigated. The most stable configurations of the optimized structures of different grafting modes (M_{13}-A, M_{13}-B, M_{13}-C, and M_{13}-D) of the Co, Cu, and Ni clusters on the SiO_2-4.6 surface are depicted in Figure 2. The interaction between the cluster and the silanol groups occurs by formation of M-O-Si bonds. However, in a few cases, nearby surface OH groups create M-OH-Si bonds. Our results show that for the optimized structure of different grafting modes, the interaction of the copper cluster to the silica surface have strongly influenced its geometric structure and introduced a new organization of atoms and consequently changes its symmetry, however, the effect is slightly lower on the clusters of Co and Ni and kept their initial symmetry. For the structure M_{13}-A, the optimized structure has 2 M-O-Si groups for both Co and Ni systems and one group for Cu system and one M-OH-Si group is established for each system. The M_{13}-B cluster is connected to the silica surfaces through two M-O-Si groups and one M-OH-Si group for cobalt system, four M-O-Si groups and 2 M-OH-Si groups for copper system, and two groups of each bonding type for the nickel system. The structure M_{13}-C shows the formation of five M-O-Si groups for cobalt and copper systems and six groups for the nickel system, and only one M-OH-Si group is established for the copper system. For the structure M_{13}-D, the optimized structure shows six M-O-Si groups established for each system and two M-OH-Si groups for the cobalt system. In addition, in a few cases, the optimized structure shows the formation of M-Si bond mainly observed for the copper and the nickel systems.

Table S1 in the Supporting Information shows the calculated equilibrium distances of the free and the adsorbed Co_{13}, Ni_{13}, and Cu_{13} clusters onto the SiO_2-3.3 and SiO_2-4.6 surfaces (distances: d_{M-M}, d_{M-O}, d_{M-OH}, and d_{M-Si}) for the most stable grafting structures. For the free M_{13} cluster, the Co-Co bond lengths are in the range of 2.40-2.69 Å and the averaged Co-Co distance is found to be 2.54 Å, while the Ni-Ni distances are in the range of 2.26-2.63 Å and the averaged is found to be 2.42 Å. However, the bond lengths of the Cu_{13} cluster are in the range of 2.34-3.19 Å and the averaged equilibrium distance is found to be 2.55 Å. For the adsorbed cluster, according to the calculated equilibrium distances reported in Table S1 in the Supporting Information, the Co-Co bond lengths of the cluster are significantly influenced by the interaction with the surface: for the structures Co_{13}-A, Co_{13}-B, and Co_{13}-C, the Co-Co bond lengths are in the range of 2.31-2.84 Å, and for the structure Co_{13}-D, are in the range of 2.33-4.23 Å, and their averaged Co-Co distance are found to be 2.53 Å and 2.63 Å, respectively. For Ni/SiO_2, the Ni-Ni bond lengths are found in the range of 2.27-3.03 Å and the averaged distance is found to be 2.43 Å. However, for Cu/SiO_2-4.6, the Cu-Cu bond lengths of the cluster are strongly influenced by the interaction with the surface: the Cu-Cu bond lengths are in the range of 2.31-5.53 Å, and 2.34-5.71 Å for Cu/SiO_2-3.3. The averaged Cu-Cu distance for the structures Cu_{13}-A, Cu_{13}-B, Cu_{13}-C, and Cu_{13}-D onto SiO_2-4.6 are found to be 2.84, 2.71, 2.78, 2.91 Å, respectively, and 2.90, 2.79, and 2.57 Å for Cu_{13}-A, Cu_{13}-B, and Cu_{13}-C onto SiO_2-3.3 Å, respectively (see Table S1 in the Supporting Information). For all cases, these distances are strongly influenced by the environment and the number of M-O-Si and M-OH-Si groups and in few cases on the number M-Si bonds.

The M-O bonds are in the range of 1.80-2.14 Å for Co/SiO_2, 1.81-2.13 Å for Ni/SiO_2, and 1.84-2.14 Å for Cu/SiO_2. However, the M-OH bond lengths are found in the range of 2.10-2.18 Å, 2.03-2.11 Å, and 2.04-2.16 Å for the supported Co, Ni, and Cu cluster on SiO_2 surface, respectively. In a few cases, the M-Si bonds are found in the range of 1.84-1.85 Å for Ni/SiO_2, and 2.45-2.46 Å for Cu/SiO_2.

3.2.2. Adsorption properties

The calculated adsorption energies of the most stable grafting structures of the transition metal clusters M_{13} on the amorphous silica surfaces (SiO_2-3.3 and SiO_2-4.6) are summarized in Table 3. The M_{13} cluster is grafted by dehydrogenation of surface silanols, following the reaction:

$$M_{13} + SiO_2(H_2)_m \rightarrow M_{13}SiO_2(H_2)_{m-\frac{n}{2}} + \frac{n}{2} \times H_2, \quad (2)$$

where n is the number of hydrogens removed from the surface (between 1 and 4) and m is the number of H_2 of the silica-surface. The adsorption energy ΔE is given by $\Delta E = E_{sys} +$

Table 3: PBE+U+D2 calculated grafting energies (in eV) for all possible grafting structures (M_{13}-A, M_{13}-B, M_{13}-C, and M_{13}-D) of different transition metal clusters (Co, Ni, and Cu) on the silica surfaces.

Model	M_{13}/SiO_2-4.6			M_{13}/SiO_2-3.3		
	Co	Ni	Cu	Co	Ni	Cu
M_{13}-A_1	-1.53	-1.37	-2.18	-1.90	-2.10	-2.27
M_{13}-A_2	-2.37	-2.69	-2.76	-2.35	-2.70	-2.64
M_{13}-A_3	-2.54	-3.15	-3.52	-2.58	-3.07	-3.22
M_{13}-B_1	-2.42	-2.95	-3.09	-2.89	-2.67	-1.67
M_{13}-B_2	-3.05	-3.88	-3.13	-4.10	-2.93	-2.92
M_{13}-B_3	-3.45	-4.26	-4.29	-8.68	-9.30	-7.77
M_{13}-C_1	-2.69	-3.44	-3.62	-3.73	-2.53	-3.44
M_{13}-C_2	-3.69	-4.10	-4.44	-4.33	-2.76	-3.88
M_{13}-C_3	-4.78	-5.69	-4.82	-4.64	-5.39	-4.31
M_{13}-D	-5.66	-	-3.88	-	-	-

$\frac{n}{2}E_{H_2} - E_{surf} - E_{clust}$, where E_{sys} is the total energy of the whole system ($M_{13}SiO_2(H_2)_{m-\frac{n}{2}}$), E_{surf} and E_{clust} are that of the free silica-surface and the free transition metal cluster M_{13}, respectively, and E_{H_2} is that of H_2's. The energies E_{surf} and E_{clust} are calculated using the same cell as that of the system in order to minimize numerical errors. The calculated grafting energies summarized in Table 3 show that all the transition metal cluster M_{13} are strongly

bonded to the amorphous silica surfaces through their oxygen atoms. In addition, we found that these energies depend strongly on the location of the cluster on the silica surface for all metals. For Co_{13}/SiO_2 system, the grafting energies of the most stable grafting structures (Co_{13}-A, Co_{13}-B, Co_{13}-C, and Co_{13}-D) on SiO_2-4.6 are found to be -2.54, -3.45, -4.78, and -5.66 eV, respectively, and on SiO_2-3.3, -2.58, -8.68, and -4.64 eV for the structures Co_{13}-A, Co_{13}-B, Co_{13}-C, respectively. For Ni_{13}/SiO_2 system, the grafting energies are found to be -3.15, -4.26, and -5.69 eV for the structures Ni_{13}-A, Ni_{13}-B, and Ni_{13}-C on SiO_2-4.6, while those on SiO_2-3.3 are found to be -3.07, -9.30, and -5.39 eV, respectively. However, the grafting energies of the most stable structures (Cu_{13}-A, Cu_{13}-B, Cu_{13}-C, and Cu_{13}-D) on SiO_2-4.6 are found to be -3.52, -4.29, -4.82, and -3.88 eV, respectively, and on SiO_2-3.3, -3.22, -7.77, -4.31 eV for the structures Cu_{13}-A, Cu_{13}-B, and Cu_{13}-C, respectively. The resulting adsorption energies of the most adsorbed transition metal clusters show that the adsorption of nickel cluster is more stronger than the cobalt than the copper ones. These values suggest also that the grafting structure M_{13}-B of all transition metal clusters on SiO_2-3.3 silica surface is the most stable. These particular configurations will be discussed in more details at the end of this section. Contrary to the adsorbed single nanoparticles, our results shown that the nickel clusters are more adsorbed than those of cobalt. However, the copper clusters are still slightly less stable than the cobalt and nickel ones. Indeed, the magnetic transition metal-silica interactions are mostly due to the strong hybridization between the open M-d shell and O-p orbitals. On the other hand, the non magnetic interactions are mostly due to the hybridization between the M-s and O-p orbitals.

A Bader analysis of the charge density has been performed for all considered systems, in order to determine the charge transfer between the transition metal cluster M_{13} and the silica surface. The charge transfer to an active site can significantly affect binding energies, and therefore catalytic activity. This is directly related to the fraction of charged sites, which evolves with the perimeter of the transition metal-support interface [60, 61]. The computed charge transfer from the amorphous silica surface to the M_{13} cluster for the most stable structures of each system are summarized in Table S2 in the Supporting Information. The resulting charge transfer from both silica surfaces SiO_2-4.6 or SiO_2-3.3 to the M_{13} cluster for the most stable structures always show that the cluster is negatively charged whatever the metal. In all cases, a sizeable charge transfer from the silica surface SiO_2-4.6 or SiO_2-3.3 is observed for the most stable structures. For the Co_{13}/SiO_2 system, the charge transfer from the SiO_2-4.6 to the cluster of the most stable structures (Co_{13}-A, Co_{13}-B, Co_{13}-C, and Co_{13}-D) are found to be 0.76, 1.28, 2.00 and 2.6 electrons, respectively, and from SiO_2-3.3, 0.78, 2.34, and 1.96 electrons for the structures Co_{13}-A, Co_{13}-B, and Co_{13}-C, respectively. A charge transfer is also observed from the silica surface SiO_2-4.6 to the nickel cluster of about 0.65, 1.27, and 1.89 electron for the structures Ni_{13}-A, Ni_{13}-B, and Ni_{13}-C, respectively. For Ni_{13}/SiO_2-3.3, the charge transfer from the surface to the cluster are found to be 0.59, 2.24, and 1.92 electron for the structures Ni_{13}-A, Ni_{13}-B, and Ni_{13}-C, respectively. However, for the Cu_{13}/SiO_2 system, the charge transfer from the SiO_2-4.6 to the cluster of the most stable structures (Cu_{13}-A, Cu_{13}-B, Cu_{13}-C, and Cu_{13}-D) are found to be 0.62, 1.25, 1.95, and 2.53 electron, respectively, and from SiO_2-3.3, 0.63, 2.03, and 1.90 electron for the structures Cu_{13}-A, Cu_{13}-B, and Cu_{13}-C, respectively. Our results show that the charge transfer to the

nickel and the copper clusters for all the most stable structures are very similar and slightly lower than that to the cobalt ones. These values depend strongly on the number of M-O-Si and M-OH-Si groups for all transition metals. Significant influence of the surface on the cluster atoms that depends on their positions relative to the surface where those in direct contact with the oxygen atoms are the most affected and relatively more less for the closer ones, while the farthest atoms from the surface are unaffected. However, a positive charge is found on the central cluster atom for all cases.

Our calculations demonstrate a better stabilization of the 13-atoms nickel clusters compared to the cobalt and the copper ones. This is confirmed by the experimental results that highlight the improvement of catalytic activity of Ni/SBA-15 catalysts [29, 26, 27]. Our results confirm the good stability and reusability of Ni-based catalysts prepared by Melt-Infiltration approach. The stabilization of 13-atoms nickel clusters on the silica surface produce sintering-resistant materials indicating their higher reducibilities and increase their catalytic activity, selectivity, and reusability [29, 26, 27].

3.2.3. Magnetic properties

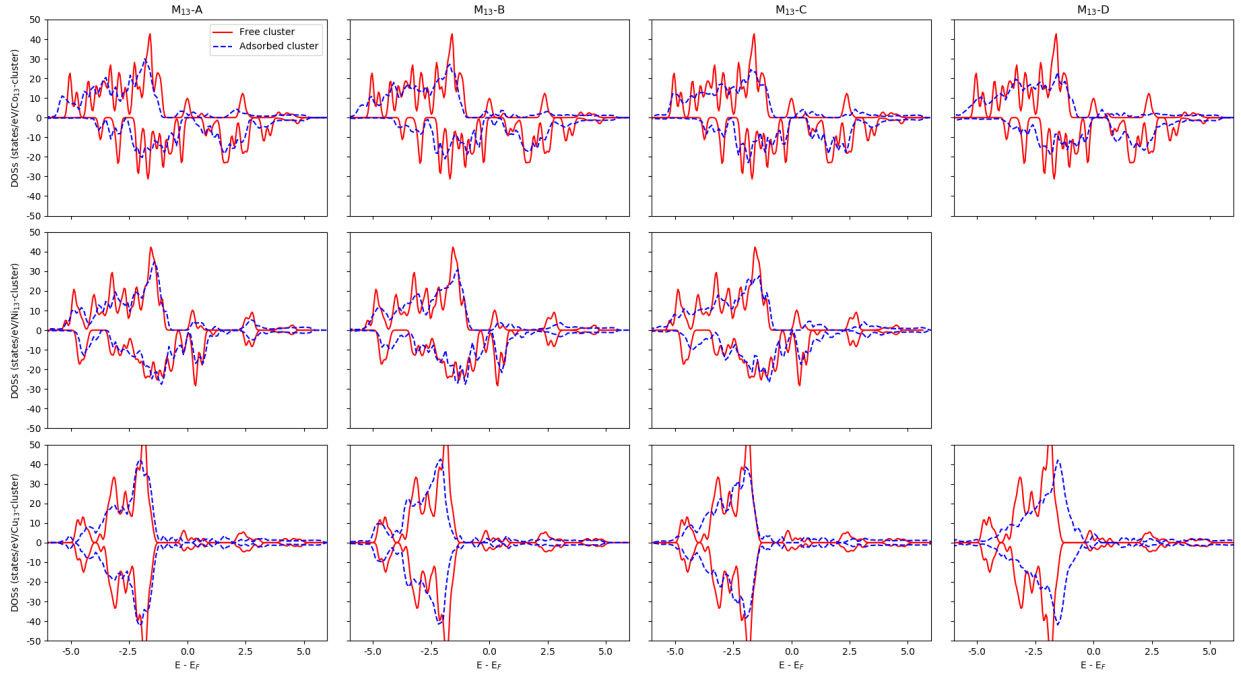

Figure 3: (Color online) PBE+U+D2 calculated spin-polarized density of states (DOSs) of the free (solid red curve) and the adsorbed (dashed blue curve) Co (upper), Ni (middle), and Cu (lower) clusters on SiO_2-4.6 for different grafting structures. The Fermi level (E_F) is the zero of energy.

The spin-polarized density of states (DOSs) of the free and the adsorbed M_{13} cluster on SiO_2 surface for the most stable geometries considered are depicted in Figure 3. In all cases, by comparing the DOSs of the free and the adsorbed transition metal cluster, we found a broadening of all peaks due to the strong hybridization of the cluster with the

silica-surface through a strong covalent bonding. A slight displacement of all peaks towards higher energies is observed for the Co_{13}/SiO_2 and the Ni_{13}/SiO_2 structures. However, for the Cu_{13}/SiO_2, the DOSs of the structure Cu_{13}-D show a large displacement of all occupied and unoccupied peaks towards the Fermi level due not only to the large number of contacts with the surface but also to the reorganization of the cluster atoms. These have also created a slight asymmetry between the spin-polarized peaks. The DOSs of Cu_{13}-B shows also a slight displacement of all peaks towards the lower energies and more less for Cu_{13}-A and Cu_{13}-C. In order to get a more precise picture of the respective stabilities of

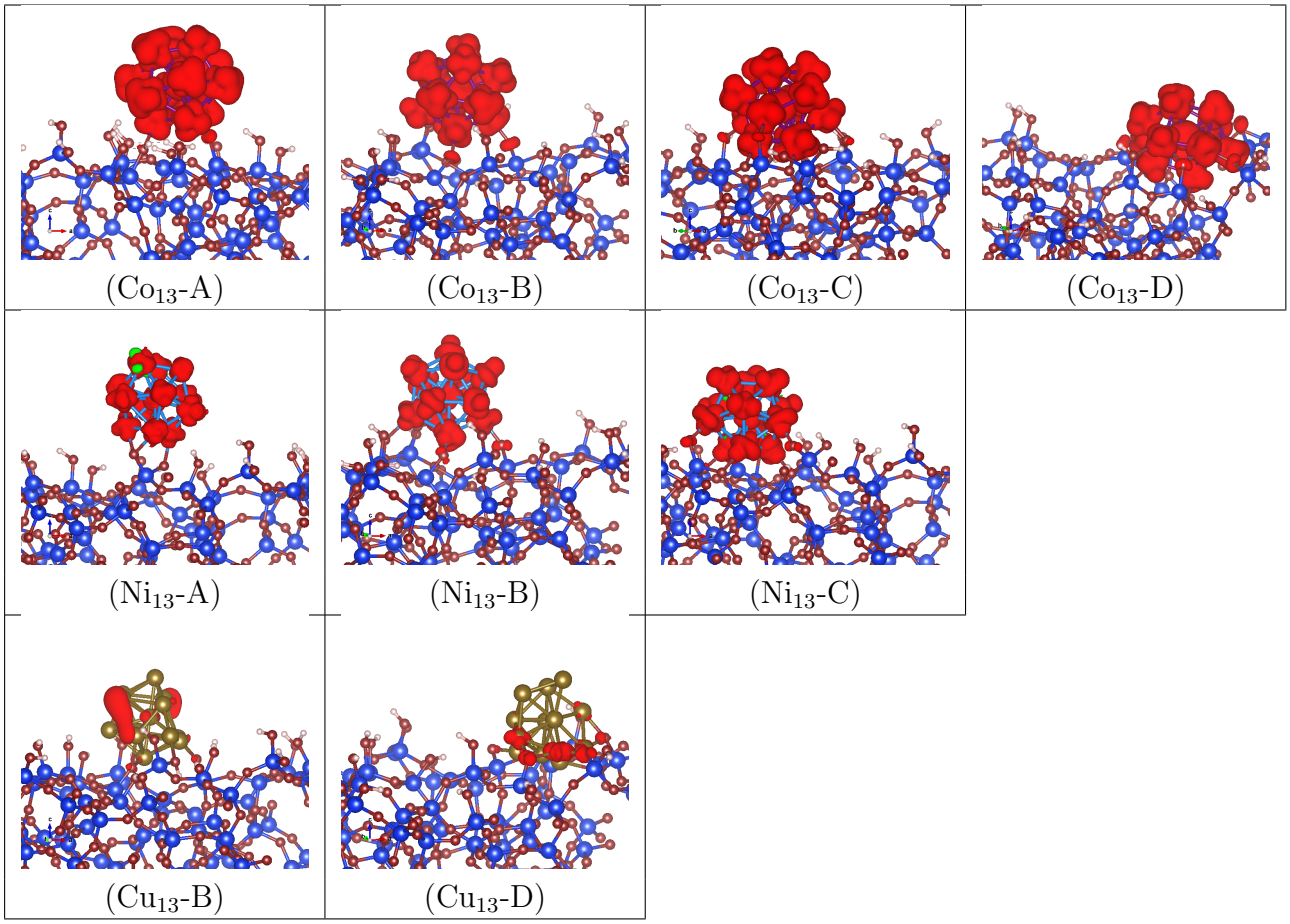

Figure 4: Isosurface plot of the magnetization density of transition metal cluster (Co: upper panels, Ni: middle panels, and Cu: lower panels) on amorphous silica surface (SiO_2-4.6). The color red represents spin up, and green represents spin down.

different grafting mode of the M_{13} cluster at the surface, we have analyzed the magnetic properties of the free and the grafted cluster for all considered grafting sites. The isosurface plot of the magnetization density of the adsorbed Co_{13} (upper panels), Ni_{13} (middle panels), and Cu_{13} (lower panels) clusters are shown in Figure 4. For all grafting structures of Co_{13}/SiO_2, a large positive magnetization density (red isosurface) is prominently observed around the cobalt atoms, and more less is also seen for the most stable structures

of Ni_{13}/SiO_2. However, for Cu_{13}/SiO_2, a small positive magnetization density seen around some copper atoms is only observed for Cu_{13}-B and Cu_{13}-D. For all these cases, there is a direct exchange between the transition metals in direct contact with the oxygen atoms due mainly to the strong hybridization between the M-*d* and O-*p* orbitals. Therefore, a small positive magnetization density has appeared on the direct contact oxygen atoms (M-O-Si), illustrating the ferromagnetic coupling between the surface and the transition metal cluster. For Co_{13}/SiO_2, the magnetic moments induced by the cobalt atoms on the contact oxygens are in the range of 0.02-0.06 μ_B, and 0.01-0.04 μ_B for those induced by the nickel atoms. For Cu_{13}/SiO_2 (Cu_{13}-D), the small magnetic moments induced on the contact oxygens are found to be 0.02 μ_B, 0.04 μ_B, and 0.04 μ_B. These values are smaller compared to those induced by the cobalt and the nickel atoms. However, for the M-OH-Si groups, the magnetic moment of the oxygen atoms is zero for all cases. Table S3 in the Supporting Information shows the calculated magnetic moments of the transition metal atom of the free and the adsorbed cluster onto the silica-surfaces (SiO_2-3.3 and SiO_2-4.6). For the free cluster, the average cobalt, nickel, and copper magnetic moments are found to be 1.92, 0.72, and 0.03 μ_B, respectively. For Co_{13}/SiO_2-4.6, the average cobalt magnetic moment are found to be 1.99, 1.95, 1.81, and 1.88 μ_B for the grafted structures Co_{13}-A, Co_{13}-B, Co_{13}-C, and Co_{13}-D, respectively, and for Co_{13}/SiO_2-3.3, 1.99, 1.88, and 1.91 for the structures Co_{13}-A, Co_{13}-B, and Co_{13}-C, respectively. The average nickel magnetic moment of the structures Ni_{13}-A, Ni_{13}-B, and Ni_{13}-C are found to be 0.75, 0.80, and 0.85 μ_B, respectively for Ni_{13}/SiO_2-4.6, and 0.77, 0.91, and 0.84 for Ni_{13}/SiO_2-3.3. Our results shown that the total cobalt magnetic moment is reduced by increasing the number of M-O-Si and M-OH-Si groups, while it is increased for Ni_{13}/SiO_2, due probably to the M-*d* - O-*p* hybridization (the open Co-*d* shell have 4 unpaired electrons, while only 2 for Ni). However, for Cu_{13}/SiO_2, the average copper magnetic moment is found to be 0.03 and 0.05 μ_B for the structures Cu_{13}-B, Cu_{13}-D, and zero for the other cases (closed Cu-*d* shell).

3.2.4. The most stable grafting model

For all transition metal models, our results show that the most stable structure (M_{13}-B) is found on the silica surface with a silanol density of 3.3 OH/nm^2. The grafting energies of this particular stable configuration are found to be -8.68 eV, -9.30 eV, and -7.77 eV for the Co_{13}, Ni_{13}, and Cu_{13} clusters, respectively (see Table 3). For all cases, the adsorption of the cluster has a strong effect on the silica surface: it has broken some Si-O-Si bonds and therefore created new silanol sites. This leads to a reorganization of the silanol groups on the silica surface and make possible to create an additional M-O-Si groups. The optimized structures of this particular stable configuration of the grafted Co_{13} (left), Ni_{13} (middle), and Cu_{13} (right) clusters are shown in Figure 5 (upper panels). For Co_{13}/SiO_2 and Ni_{13}/SiO_2, the optimized structure shows the formation of 6 M-O-Si bonds, that were initially grafted with only two M-O-Si groups. However, for Cu_{13}/SiO_2, due to the deformation of the cluster after adsorption, the optimized structure shows that Cu_{13} make 6 Cu-O-Si and 2 Cu-Si bonds with the silica surface. The Cu atom binds to the silica surface through direct coupling of the singly occupied Si sp^3 dangling bond and Cu 4s orbitals. The resulting bonding orbital has substantial covalent character with distance value in the range of 2.45- 2.46 Å (see Table S1)

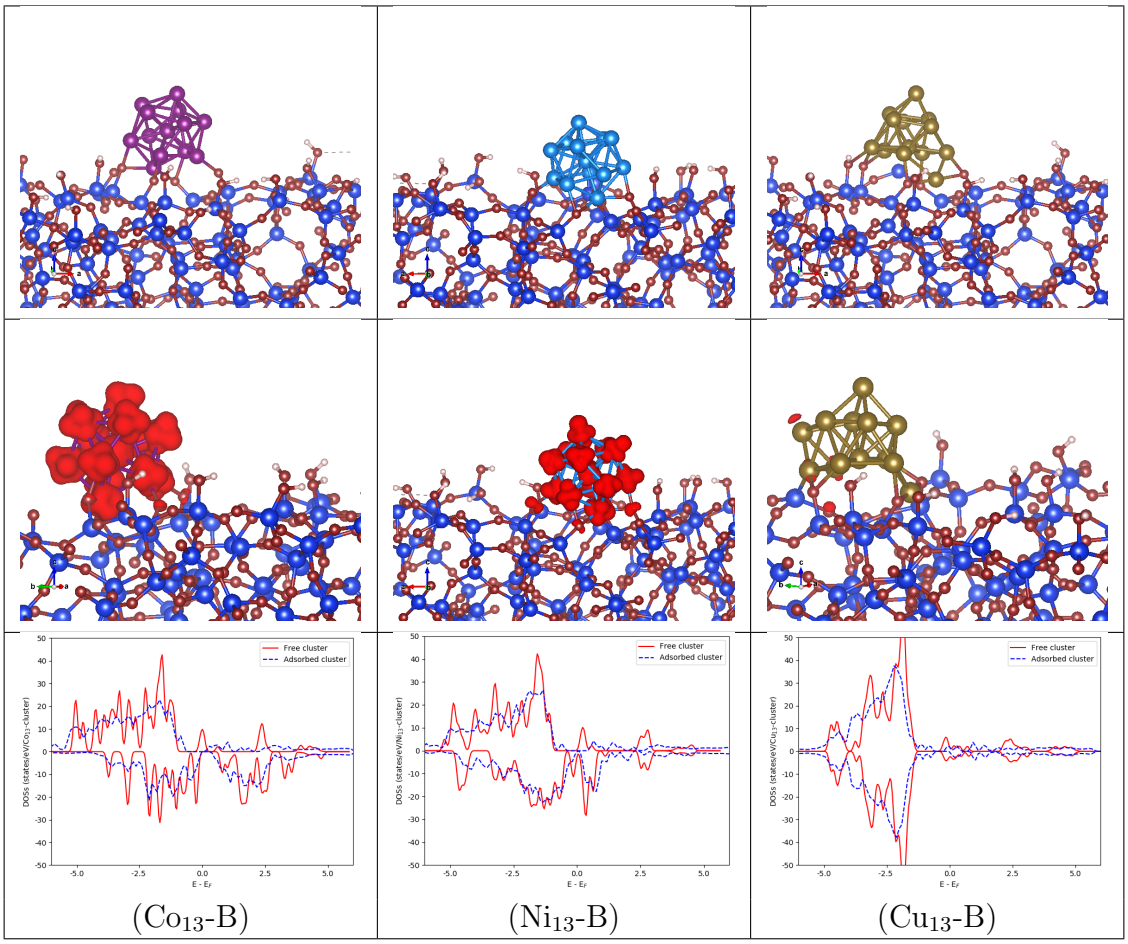

Figure 5: Upper panels show the optimized structures of the most stable configuration of supported transition metal clusters (Co: left, Ni: middle, and Cu: right) on SiO_2-3.3 surface. The middle and the lower panels show the corresponding magnetization density and the total DOSs, respectively.

in agreement with most of reported distance computed within different theoretical methods [62, 63]. While the XAFS-derived Cu-Si distance is in the range of 2.6 to 3.5 Å [64]. This leads to the reduction of its grafting energy (-7.77 eV) compared to those of the cobalt and nickel systems. This effect is clearly observed on the spin-polarized density of states for all metals shown in Figure 5 (lower panels). Our results show a broadening and displacement of all occupied and unoccupied states (spin-up and spin-down) towards higher energies for Co_{13}/SiO_2 and Ni_{13}/SiO_2 and to lower energies for Cu_{13}/SiO_2 system. A comparison between the electronic levels of the partial DOSs of an interacted atom of the free and the adsorbed Co, Ni, and Cu clusters on SiO_2-3.3 for the most grafting structures (M_{13}-B structures) are shown in Figure S1 in the Supporting Information. For different clusters, the strong effect of the silica surface appears clearly on the *d*-states (broadening and displacement of the occupied and unoccupied states). This confirms the strong hybridization between the M-*d* and O-*p* orbitals. This effect is observed also on the magnetic properties, where the total magnetic moment is reduced from 25.03 μ_B to 24.44 μ_B for Co_{13}/SiO_2, while for Ni_{13}/SiO_2,

is strongly increased from 9.42 μ_B to 11.80 μ_B, which are probably due to the number of unpaired electrons of the open M-*d* shell (Co($3d^6$), Ni($3d^8$)). However, for Cu_{13}/SiO_2, the total magnetic moment is found to be 0.36 μ_B compared to zero magnetic moment of all atoms of the free cluster may be due to a slight hybridization between the closed Cu-*d* shell and O-*p* orbitals. A large charge transfer from the silica surface to the cluster for all transition metals is observed: from 0.76 to 2.34 electron for Co_{13}/SiO_2, from 0.65 to 2.24 electron for Ni_{13}/SiO_2, and for Cu_{13}/SiO_2 from 0.62 to 2.03 electron.

4. Conclusions

(Co, Ni, and Cu)@amorphous silica are attractive materials for a wide range of applications. However, little is known regarding the grafting modes of those transition metals on the silica surfaces. Different geometrical configurations of supported transition metal monomers and clusters on various amorphous silica surfaces at different locations were systematically investigated within the PBE+U+D2 approximation. For supported transition metal monomers, our results show that the most stable structure is predicted to be the bridge grafting mode for Co/SiO_2 and Ni/SiO_2 and the top site for Cu/SiO_2 systems. Their grafting energies are in the order $\Delta E_{Co/SiO_2}$ (-3.18 eV) < $\Delta E_{Ni/SiO_2}$ (-2.42 eV) < $\Delta E_{Cu/SiO_2}$ (-2.03 eV), showing that the supported single cobalt atom is the most stable structure. It is shown that the geometry, energetic stability and magnetic properties of supported transition metal nanoclusters on silica surfaces depend strongly on the number of M-O-Si and M-OH-Si bonds. Among the three types of M_{13} clusters considered, the strong distortion is observed for adsorbed Cu_{13}, where the Cu-Cu distance varies from 2.31 Å to 5.53 Å and consequently strong reduction of the symmetry, as compared to that of the adsorbed Co_{13} and Ni_{13} on the silica surface. Contrary to the adsorbed single transition metal atoms, the adsorption energies of the adsorbed clusters are in the order $\Delta E_{Ni/SiO_2}$ (-9.30 eV) < $\Delta E_{Co/SiO_2}$ (-8.68 eV) < $\Delta E_{Cu/SiO_2}$ (-7.77 eV), showing that adsorbed nickel clusters are the most stable structure. The magnetic moements of the adsorbed Co_{13} clusters on amorphous silica surface are found to be reduced with respect to their corresponding free clusters, while it is increased for Ni_{13}/SiO_2 system. Our calculations show a large charge transfer from the silica surface to the cluster for all transition metals of about 2 to 3 electrons. Our work opens the path towards the investigation of adsorption or catalytic process using amorphous silica.

Supporting Information

See Supporting Information for additional tables, including the calculated equilibrium distance (in Å) d_{M-M}, d_{M-O}, d_{M-OH}, and d_{M-Si} and the magnetic moments of all atoms of the free and the grafted transition metal (Co, Ni, and Cu) cluster on SiO_2-4.6 or SiO_2-3.3, the computed charge transfer per atom (in e^-) from both silica surfaces to different transition metal cluster for the most stable grafting structures (M_{13}-A, M_{13}-B, M_{13}-C, and M_{13}-D) using the PBE+U+D2 approximation, and the calculated partial spin-polarized density of states of an interacted atom of the free and the adsorbed Co, Ni, and Cu clusters on SiO_2-3.3 for the most grafting structures (M_{13}-B structures).

Acknowledgments

We would like to acknowledge fruitful discussion with Andreea Pasc, Nadia Canilho, and Younes Bouizi. This work was performed using the HPC Mesocenter "Explor" and GENCI. S. G. is grateful to the program Lorraine University of Excellence for funding this work with the Lignin program. The authors acknowledge financial support through the COMETE project (COnception in silico de Matériaux pour l'EnvironmenT et l'Energie) cofunded by the European Union under the program "FEDER-FSE Lorraine et Massif des Voges 2014-2020".

References

[1] D. Kim, I. Wachs, Surface chemistry of supported chromium oxide catalysts, J. Catal. 142 (1) (1993) 166 – 171. doi:https://doi.org/10.1006/jcat.1993.1198.

[2] A. B. Gaspar, C. A. C. Perez, L. C. Dieguez, Characterization of Cr/SiO_2 catalysts and ethylene polymerization by XPS, Appl. Surf. Sci. 252 (4) (2005) 939–949. doi:10.1016/j.apsusc.2005.01.031.

[3] M. Banares, J. Fierro, J. Moffat, The partial oxidation of methane on MoO_3/SiO_2 catalysts: Influence of the molybdenum content and type of oxidant, J. Catal. 142 (2) (1993) 406 – 417. doi:https://doi.org/10.1006/jcat.1993.1218.

[4] G. S. Pozan, A. Tavman, I. Boz, Dehydroisomerization of n-butane over Cr/SiO_2, Chem. Eng. J. 143 (1) (2008) 180 – 185. doi:https://doi.org/10.1016/j.cej.2008.04.004.

[5] K. C. Szeto, B. Loges, N. Merle, N. Popoff, A. Quadrelli, H. Jia, E. Berrier, A. De Mallmann, L. Delevoye, R. M. Gauvin, M. Taoufik, Vanadium oxo organometallic species supported on silica for the selective non-oxidative dehydrogenation of propane, Organometallics 32 (21) (2013) 6452–6460. doi:10.1021/om400795s.

[6] X. Li, P. Wang, H. Wang, C. Li, Effects of the state of Co species in Co/Al_2O_3 catalysts on the catalytic performance of propane dehydrogenation, Appl. Surf. Sci. 441 (2018) 688–693. doi:10.1016/j.apsusc.2018.02.024.

[7] B. M. Weckhuysen, I. E. Wachs, R. A. Schoonheydt, Surface chemistry and spectroscopy of chromium in inorganic oxides, Chem. Rev. 96 (8) (1996) 3327–3350. doi:10.1021/cr940044o.

[8] L. Liotta, A. Venezia, G. Pantaleo, G. Deganello, M. Gruttadauria, R. Noto, Chromia on silica and zirconia oxides as recyclable oxidizing system: structural and surface characterization of the active chromium species for oxidation reaction, Catal. Today 91-92 (2004) 231 – 236. doi:https://doi.org/10.1016/j.cattod.2004.03.050.

[9] J. Guo, C. Lin, C. Jiang, P. Zhang, Review on noble metal-based catalysts for formaldehyde oxidation at room temperature, Appl. Surf. Sci. 475 (2019) 237–255. doi:10.1016/j.apsusc.2018.12.238.

[10] M. Badawi, J. Paul, S. Cristol, E. Payen, Y. Romero, F. Richard, S. Brunet, D. Lambert, X. Portier, A. Popov, E. Kondratieva, J. Goupil, J. E. Fallah, J. Gilson, L. Mariey, A. Travert, F. Mauge, Effect of water on the stability of Mo and CoMo hydrodeoxygenation catalysts: A combined experimental and DFT study, J. Catal. 282 (1) (2011) 155 – 164. doi:https://doi.org/10.1016/j.jcat.2011.06.006.

[11] R. Olcese, M. Bettahar, D. Petitjean, B. Malaman, F. Giovanella, A. Dufour, Gas-phase hydrodeoxygenation of guaiacol over Fe/SiO_2 catalyst, Appl. Catal. B: Environ. 115-116 (2012) 63 – 73". doi:https://doi.org/10.1016/j.apcatb.2011.12.005.

[12] R. N. Olcese, J. Francois, M. M. Bettahar, D. Petitjean, A. Dufour, Hydrodeoxygenation of guaiacol, a surrogate of lignin pyrolysis vapors, over iron based catalysts: Kinetics and modeling of the lignin to aromatics integrated process, Energy Fuels 27 (2) (2013) 975–984. doi:10.1021/ef301971a.

[13] R. N. Olcese, G. Lardier, M. Bettahar, J. Ghanbaja, S. Fontana, V. Carré, F. Aubriet, D. Petitjean, A. Dufour, Aromatic chemicals by iron-catalyzed hydrotreatment of lignin pyrolysis vapor, ChemSusChem 6 (8) (2013) 1490–1499. doi:10.1002/cssc.201300191.

[14] Badawi, M., Paul, J.-F., Payen, E., Romero, Y., Richard, F., Brunet, S., Popov, A., Kondratieva, E., Gilson, J.-P., Mariey, L., Travert, A., Maugé, F., Hydrodeoxygenation of phenolic compounds by sulfided (Co)Mo/Al_2O_3 catalysts, a combined experimental and theoretical study, Oil Gas Sci. Technol. - Rev. IFP Energies nouvelles 68 (2013) 829–840. doi:10.2516/ogst/2012041.

[15] Z. Zhang, M. Tang, J. Chen, Effects of P/Ni ratio and Ni content on performance of γ-Al_2O_3-supported nickel phosphides for deoxygenation of methyl laurate to hydrocarbons, Appl. Surf. Sci. 360 (2016) 353–364. doi:10.1016/j.apsusc.2015.10.182.

[16] Z. Nie, Z. Zhang, J. Chen, Effect of Ni and noble metals (Ru, Pd and Pt) on performance of bi-functional MoP/SiO_2 for hydroconversion of methyl laurate, Appl. Surf. Sci. 420 (2017) 511–522. doi:10.1016/j.apsusc.2017.05.173.

[17] Z. Gao, F. Liu, L. Wang, F. Luo, Highly efficient transfer hydrodeoxygenation of vanillin over Sn^{4+}-induced highly dispersed Cu-based catalyst, Appl. Surf. Sci. 480 (2019) 548–556. doi:10.1016/j.apsusc.2019.02.219.

[18] C. Chizallet, P. Raybaud, Density functional theory simulations of complex catalytic materials in reactive environments: beyond the ideal surface at low coverage, Catal. Sci. Technol. 4 (2014) 2797–2813. doi:10.1039/C3CY00965C.

[19] S. Simonetti, A. D. Company, E. Pronsato, A. Juan, G. Brizuela, A. Lam, Density functional theory based-study of 5-fluorouracil adsorption on β-cristobalite (111) hydroxylated surface: The importance of H-bonding interactions, Appl. Surf. Sci. 359 (2015) 474 – 479. doi:https://doi.org/10.1016/j.apsusc.2015.10.147.

[20] A. B. Schvval, A. Juan, G. F. Cabeza, Theoretical study of the role of the interface of Ag_4 nanoclusters deposited on TiO_2(110) and TiO_2(101), Appl. Surf. Sci. 490 (2019) 343 – 351. doi:https://doi.org/10.1016/j.apsusc.2019.05.291.

[21] H. Guesmi, R. Grybos, J. Handzlik, F. Tielens, Characterization of molybdenum monomeric oxide species supported on hydroxylated silica: a DFT study, Phys. Chem. Chem. Phys. 16 (2014) 18253–18260. doi:10.1039/C4CP02296C.

[22] M. Gierada, P. Michorczyk, F. Tielens, J. Handzlik, Reduction of chromia-silica catalysts: A molecular picture, J. Catal. 340 (2016) 122 – 135. doi:https://doi.org/10.1016/j.jcat.2016.04.022.

[23] B. R. Goldsmith, B. Peters, J. K. Johnson, B. C. Gates, S. L. Scott, Beyond ordered materials: Understanding catalytic sites on amorphous solids, ACS Catal. 7 (11) (2017) 7543–7557. doi:10.1021/acscatal.7b01767.

[24] T. Siodla, I. Sobczak, M. Ziolek, F. Tielens, Theoretical and experimental insight into zinc loading on mesoporous silica, Micropor. Mesopor. Mat. 256 (2018) 199 – 205. doi:https://doi.org/10.1016/j.micromeso.2017.08.008.

[25] F. Tielens, M. Gierada, J. Handzlik, M. Calatayud, Characterization of amorphous silica based catalysts using DFT computational methods, Catal. Today In Press (2019) Corrected Proof. doi:https://doi.org/10.1016/j.cattod.2019.03.062.

[26] C. Ciotonea, I. Mazilu, B. Dragoi, C. Catrinescu, E. Dumitriu, A. Ungureanu, H. Alamdari, S. Petit, S. Royer, Confining for stability: Heterogeneous catalysis with Transition Metal (Oxide) Nanoparticles confined in the secondary pore network of mesoporous scaffolds, ChemNanoMat 3 (4) (2017) 233–237. doi:10.1002/cnma.201700014.

[27] C. Ciotonea, B. Dragoi, A. Ungureanu, C. Catrinescu, S. Petit, H. Alamdari, E. Marceau, E. Dumitriu, S. Royer, Improved dispersion of transition metals in mesoporous materials through a polymer-assisted melt infiltration method, Catal. Sci. Technol. 7 (2017) 5448–5456. doi:10.1039/C7CY00963A.

[28] B. Dragoi, I. Mazilu, A. Chirieac, C. Ciotonea, A. Ungureanu, E. Marceau, E. Dumitriu, S. Royer, Highly dispersed copper (oxide) nanoparticles prepared on SBA-15 partially occluded with the P123 surfactant: toward the design of active hydrogenation catalysts, Catal. Sci. Technol. 7 (2017) 5376–5385. doi:10.1039/C7CY01015J.

[29] S. Chen, C. Ciotonea, A. Ungureanu, E. Dumitriu, C. Catrinescu, R. Wojcieszak, F. Dumeignil, S. Royer, Preparation of nickel (oxide) nanoparticles confined in the secondary pore network of mesoporous scaffolds using melt infiltration, Catal. Today 334 (2019) 48 – 58.

doi:https://doi.org/10.1016/j.cattod.2019.01.064.
[30] M. Badawi, L. Vivier, G. Perot, D. Duprez, Promoting effect of cobalt and nickel on the activity of hydrotreating catalysts in hydrogenation and isomerization of olefins, J. Mol. Catal. A Chem. 293 (1) (2008) 53 – 58. doi:https://doi.org/10.1016/j.molcata.2008.07.006.
[31] M. Badawi, L. Vivier, D. Duprez, Kinetic study of olefin hydrogenation on hydrotreating catalysts, J. Mol. Catal. A Chem. 320 (1) (2010) 34 – 39. doi:https://doi.org/10.1016/j.molcata.2009.12.012.
[32] W. Hu, L. Mei, H. Li, Simulation of ground state structure of nickel clusters (n $\leq$ 40), Solid State Commun. 100 (1996) 129 – 131. doi:https://doi.org/10.1016/0038-1098(96)00396-1.
[33] M. Kabir, A. Mookerjee, A. K. Bhattacharya, Structure and stability of copper clusters: A tight-binding molecular dynamics study, Phys. Rev. A 69 (2004) 043203. doi:10.1103/PhysRevA.69.043203.
[34] Z. Xie, Q.-M. Ma, Y. Liu, Y.-C. Li, First-principles study of the stability and Jahn-Teller distortion of nickel clusters, Phys. Lett. A 342 (2005) 459 – 467. doi:https://doi.org/10.1016/j.physleta.2005.05.067.
[35] G. R. S.D. Borisova, E. Chulkov, Structure and vibrational properties of cobalt clusters (n $\leq$ 20), Phys. Solid State 52 (2010) 838–843. doi:https://doi.org/10.1134/S106378341004027X.
[36] M. S. Stave, A. E. DePristo, The structure of nin and pdn clusters: 4$\leq$n$\leq$23, J. Chem. Phys. 97 (5) (1992) 3386–3398. doi:10.1063/1.462975.
[37] H. Jabraoui, E. Hessou, S. Chibani, L. Cantrel, S. Lebègue, M. Badawi, Adsorption of volatile organic and iodine compounds over silver-exchanged mordenites: A comparative periodic DFT study for several silver loadings, Appl. Surf. Sci. 485 (2019) 56 – 63. doi:https://doi.org/10.1016/j.apsusc.2019.03.282.
[38] Y. Berro, S. Gueddida, S. Lebègue, A. Pasc, N. Canilho, M. Kassir, F. E. H. Hassan, M. Badawi, Atomistic description of phenol, CO and H_2O adsorption over crystalline and amorphous silica surfaces for hydrodeoxygenation applications, Appl. Surf. Sci. 494 (2019) 721 – 730. doi:https://doi.org/10.1016/j.apsusc.2019.07.216.
[39] S. Chempath, Y. Zhang, A. T. Bell, DFT studies of the structure and vibrational spectra of isolated molybdena species supported on silica, J. Phys. Chem. C 111 (3) (2007) 1291–1298. doi:10.1021/jp064741j.
[40] G. Kresse, J. Furthmüller, Efficient iterative schemes for ab initio total-energy calculations using a plane-wave basis set, Phys. Rev. B 54 (1996) 11169–11186. doi:10.1103/PhysRevB.54.11169.
[41] P. E. Blöchl, Projector augmented-wave method, Phys. Rev. B 50 (1994) 17953–17979. doi:10.1103/PhysRevB.50.17953.
[42] J. P. Perdew, K. Burke, M. Ernzerhof, Generalized gradient approximation made simple, Phys. Rev. Lett. 77 (1996) 3865–3868. doi:10.1103/PhysRevLett.77.3865.
[43] V. I. Anisimov, F. Aryasetiawan, A. I. Lichtenstein, First-principles calculations of the electronic structure and spectra of strongly correlated systems: the LDA+U method, J. Phys. Condens. Matter 9 (4) (1997) 767–808. doi:10.1088/0953-8984/9/4/002.
[44] O. Bengone, M. Alouani, P. Blöchl, J. Hugel, Implementation of the projector augmented-wave LDA+U method: Application to the electronic structure of nio, Phys. Rev. B 62 (2000) 16392–16401. doi:10.1103/PhysRevB.62.16392.
[45] S. Grimme, Semiempirical GGA-type density functional constructed with a long-range dispersion correction, J. Comput. Chem. 27 (15) (2006) 1787–1799. doi:10.1002/jcc.20495.
[46] T. Bucko, J. Hafner, S. Lebègue, J. G. Angyán, Improved description of the structure of molecular and layered crystals: Ab initio DFT calculations with van der Waals corrections, J. Phys. Chem. A 114 (43) (2010) 11814–11824. doi:10.1021/jp106469x.
[47] L. T. Zhuravlev, Concentration of hydroxyl groups on the surface of amorphous silicas, Langmuir 3 (3) (1987) 316–318. doi:10.1021/la00075a004.
[48] A. P. Legrand, The Surface Properties of Silicas, Wiley, 1998.
URL https://www.wiley.com/en-us/The+Surface+Properties+of+Silicas-p-9780471953326
[49] J. L. Blin, C. Carteret, Investigation of the silanols groups of mesostructured silica prepared using a fluorinated surfactant: Influence of the hydrothermal temperature, J. Phys. Chem. C 111 (39) (2007) 14380–14388. doi:10.1021/jp072369h.
[50] F. Tielens, C. Gervais, J. F. Lambert, F. Mauri, D. Costa, Ab initio study of the hydroxylated surface of

amorphous silica: A representative model, Chem. Mater. 20 (2008) 3336–3344. doi:10.1021/cm8001173.
[51] M. Gierada, I. Petit, J. Handzlik, F. Tielens, Hydration in silica based mesoporous materials: a DFT model, Phys. Chem. Chem. Phys. 18 (2016) 32962–32972. doi:10.1039/C6CP05460A.
[52] Y. Berro, S. Gueddida, Y. Bouizi, C. Bellouard, E.-E. Bendeif, A. Gansmuller, A. Celzard, V. Fierro, D. Ihiawakrim, O. Ersen, M. Kassir, F. E. H. Hassan, S. Lebegue, M. Badawi, N. Canilho, A. Pasc, Imprinting isolated single iron atoms onto mesoporous silica by templating with metallosurfactants, J. Colloid Interf. Sci. 573 (2020) 193 – 203. doi:https://doi.org/10.1016/j.jcis.2020.03.095.
[53] A. Comas-Vives, Amorphous SiO_2 surface models: energetics of the dehydroxylation process, strain, ab initio atomistic thermodynamics and IR spectroscopic signatures, Phys. Chem. Chem. Phys. 18 (2016) 7475–7482. doi:10.1039/C6CP00602G.
[54] E. Kim, A. Mohrland, P. F. Weck, T. Pang, K. R. Czerwinski, D. Tomànek, Magic numbers in small iron clusters: A first-principles study, Chem. Phys. Lett. 613 (2014) 59 – 63. doi:https://doi.org/10.1016/j.cplett.2014.08.056.
[55] K. G. Steenbergen, N. Gaston, Ultra stable superatomic structure of doubly magic Ga_{13} and $Ga_{13}Li$ electrolyte, Nanoscale 12 (2020) 289–295. doi:10.1039/C9NR06959C.
[56] C. Di Paola, L. Pavan, R. D'Agosta, F. Baletto, Structural stability and uniformity of magnetic Pt_{13} nanoparticles in NaY zeolite, Nanoscale 9 (2017) 15658–15665. doi:10.1039/C7NR03533K.
[57] R. F. W. Bader, Principle of stationary action and the definition of a proper open system, Phys. Rev. B 49 (1994) 13348–13356. doi:10.1103/PhysRevB.49.13348.
[58] E. Sanville, S. D. Kenny, R. Smith, G. Henkelman, Improved grid-based algorithm for bader charge allocation, J. Comput. Chem. 28 (5) (2007) 899–908. doi:10.1002/jcc.20575.
[59] E. Aubert, S. Lebègue, M. Marsman, T. T. T. Bui, C. Jelsch, S. Dahaoui, E. Espinosa, J. G. Angyán, Periodic projector augmented wave density functional calculations on the hexachlorobenzene crystal and comparison with the experimental multipolar charge density model, J. Phys. Chem. A 115 (50) (2011) 14484–14494. doi:10.1021/jp206623x.
[60] W. T. Wallace, R. L. Whetten, Carbon monoxide adsorption on selected gold clusters: Highly size-dependent activity and saturation compositions, J. Phys. Chem. B 104 (47) (2000) 10964–10968. doi:10.1021/jp002889b.
[61] C. S. Ewing, G. Veser, J. J. McCarthy, D. S. Lambrecht, J. K. Johnson, Predicting catalyst-support interactions between metal nanoparticles and amorphous silica supports, Surf. Sci. 652 (2016) 278 – 285. doi:https://doi.org/10.1016/j.susc.2016.03.004.
[62] N. Lopez, G. Pacchioni, F. Maseras, F. Illas, Hybrid quantum-mechanical and molecular mechanics study of Cu atoms deposition on SiO_2 surface defects, Chem. Phys. Lett. 294 (6) (1998) 611 – 618. doi:https://doi.org/10.1016/S0009-2614(98)00907-5.
[63] T.-R. Shan, B. D. Devine, S. R. Phillpot, S. B. Sinnott, Molecular dynamics study of the adhesion of Cu/SiO_2 interfaces using a variable-charge interatomic potential, Phys. Rev. B 83 (2011) 115327. doi:10.1103/PhysRevB.83.115327.
[64] XAFS spectroscopy study of Cu(II) sorption on amorphous SiO_2 and γ-Al_2O_3: Effect of substrate and time on sorption complexes, Journal of Colloid and Interface Science 208 (1) (1998) 110–128. doi:https://doi.org/10.1006/jcis.1998.5678.

Highlights:

- NP/silica catalysts are potentially active and selective for a large panel of applications.
- Grafting mechanisms of transition metal species (Co, Ni, Cu) under various forms on amorphous silica surfaces.
- Transition metal clusters are strongly bonded to the surface through M-O-Si and M-OH-Si bonds.
- A Large charge transfer due to the strong effect of the transition metal cluster on the silica surface.

Graphical Abstract

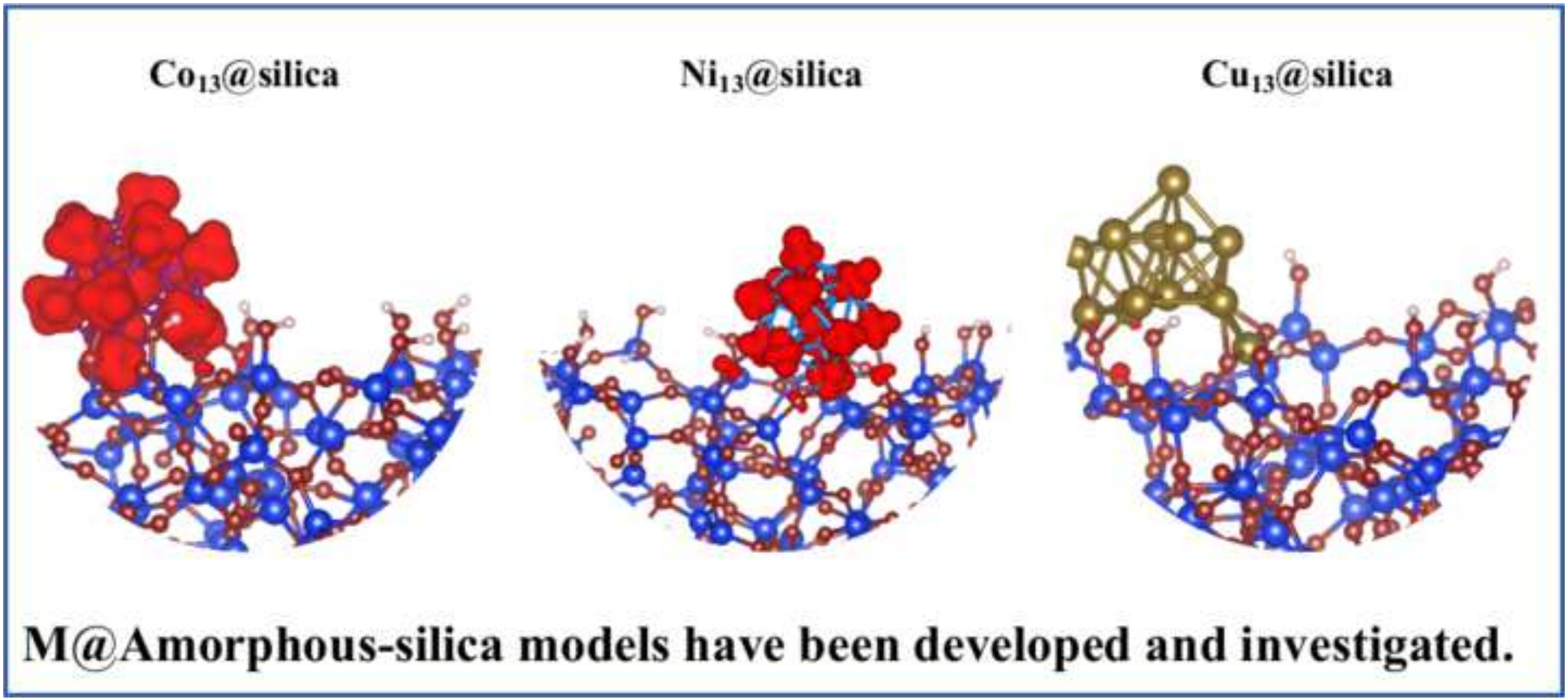

GraphicalAbstract.pdf

CrediT author statement:

Saber Gueddida: Conceptualization, Writing- Original draft preparation, Visualization, Investigation, Writing- Review & Editing, Formal Analysis. **Sébastien Lebègue:** Supervision, Resources, Conceptualization, Validation, Writing – Review & Editing, Project administration, Funding acquisition, Conceptualization. **Michael Badawi:** Supervision, Resources, Conceptualization, Validation, Writing – Review & Editing, Project administration, Funding acquisition, Conceptualization.

Declaration of interests

☒ The authors declare that they have no known competing financial interests or personal relationships that could have appeared to influence the work reported in this paper.

☐The authors declare the following financial interests/personal relationships which may be considered as potential competing interests:

The authors declare that they have no known competing financial interests or personal relationships that could have appeared to influence the work reported in this paper.